NEOPLASIA
www.neoplasia.com

Volume 11 Number 1 January 2009 pp. 77–86 77

Glioblastoma Inhibition by Cell Surface Immunoglobulin Protein EWI-2, *In Vitro* and *In Vivo*[1,2]

Tatiana V. Kolesnikova[*,†], Alexander R. Kazarov[*,†], Madeleine E. Lemieux[†,‡], Marc A. Lafleur[*,†], Santosh Kesari[§,¶], Andrew L. Kung[†,‡] and Martin E. Hemler[*,†]

*Department of Cancer Immunology and AIDS, Dana-Farber Cancer Institute, Boston, MA, USA; [†]Department of Pathology, Harvard Medical School, Boston, MA, USA; [‡]Department of Pediatric Oncology, Dana-Farber Cancer Institute, Boston, MA, USA; [§]Departments of Cancer Biology and Medical Oncology, Dana-Farber Cancer Institute, Boston, MA, USA; [¶]Department of Neurology, Brigham and Women's Hospital, Boston, MA, USA

Abstract

EWI-2, a cell surface IgSF protein, is highly expressed in normal human brain but is considerably diminished in glioblastoma tumors and cell lines. Moreover, loss of EWI-2 expression correlated with a shorter survival time in human glioma patients, suggesting that EWI-2 might be a natural inhibitor of glioblastoma. In support of this idea, EWI-2 expression significantly impaired both ectopic and orthotopic tumor growth in nude mice *in vivo*. *In vitro* assays provided clues regarding EWI-2 functions. Expression of EWI-2 in T98G and/or U87-MG malignant glioblastoma cell lines failed to alter two-dimensional cell proliferation but inhibited glioblastoma colony formation in soft agar and caused diminished cell motility and invasion. At the biochemical level, EWI-2 markedly affects the organization of four molecules (tetraspanin proteins CD9 and CD81 and matrix metalloproteinases MMP-2 and MT1-MMP), which play key roles in the biology of astrocytes and gliomas. EWI-2 causes CD9 and CD81 to become more associated with each other, whereas CD81 and other tetraspanins become less associated with MMP-2 and MT1-MMP. We propose that EWI-2 inhibition of glioblastoma growth *in vivo* is at least partly explained by the capability of EWI-2 to inhibit growth and/or invasion *in vitro*. Underlying these functional effects, EWI-2 causes a substantial molecular reorganization of multiple molecules (CD81, CD9, MMP-2, and MT1-MMP) known to affect proliferation and/or invasion of astrocytes and/or glioblastomas.

Neoplasia (2009) 11, 77–86

Introduction

Malignant gliomas constitute most primary brain tumors. Along with high proliferative capacity, invasiveness, and resistance to conventional therapies, they are characterized by a progressive rise in the number and nature of cytogenetic aberrations [1]. For multiple reasons, we considered that EWI-2, a cell surface transmembrane protein in the immunoglobulin superfamily [2], might affect glioma tumor biology. First, mRNA for EWI-2 is more elevated in brain than in any other adult human tissue [2]. Second, EWI-2 affects the motility and morphology of multiple distinct tumor cell types [3–5]. Third, EWI-2 associates closely with two proteins (tetraspanins CD9 and CD81) that have previously been linked to astrocyte-astrocytoma tumor progression and/or proliferation. Whereas CD9 expression correlates with

Abbreviations: EWI-2 and EWI-F, cell surface immunoglobulin superfamily proteins containing conserved "Glu-Trp-Ile" motifs; MT1-MMP, membrane type 1 matrix metalloproteinase; MMP-2, matrix metalloproteinase 2; TEM, tetraspanin-enriched microdomain

Address all correspondence to: Martin E. Hemler, Dana-Farber Cancer Institute, Rm D1430, 44 Binney Street, Boston, MA 02115. E-mail: martin_hemler@dfci.harvard.edu

[1]This work was supported by grants from the National Institutes of Health (GM38903, CA42368) to M.E.H., Ruth L. Kirschstein National Research Service Award (T32) to T.V.K., Sidney Kimmel Foundation grant to A.L.K., Canadian Institutes of Health Research Fellowship to M.A.L, and National Institutes of Health K08 (K08CA124804) and Sontag Foundation Distinguished Scientist Award to S.K.

[2]This article refers to supplementary materials, which are designated by Table W1 and Figures W1 to W6 and are available online at www.neoplasia.com.

Received 16 September 2008; Revised 22 October 2008; Accepted 23 October 2008

DOI 10.1593/neo.81180

astrocytic tumor malignancy [6], CD81 is highly expressed on normal astrocytes and regulates neuron-induced astrocytic cell cycle arrest and differentiation [7]. Consequently, CD81 null mice in mixed genetic backgrounds have enlarged brains owing to more astrocytes [8]. Furthermore, CD9 affects epidermal growth factor receptor ligand binding activities of the membrane-bound forms of transforming growth factor α and heparin-binding EGF-like growth factor [9,10], two molecules that contribute to human malignant glioma cell growth, most likely through juxtacrine and autocrine mechanisms [6,11,12].

Tetraspanins such as CD9 and CD81 influence motility and proliferation of normal cells and the metastatic functions and tumorigenicity of malignant cells [13,14]. To accomplish these actions, they do not typically serve as cell surface receptors, but rather function, together with laterally associated partner proteins (e.g., EWI-2, integrins, other tetraspanins), in the context of tetraspanin-enriched microdomains (TEMs) [15] on the cell surface. Changes in the protein content of TEMs can be seen as cells differentiate and/or progress toward a malignant state [16,17]. EWI-2, a major protein partner for CD9 and CD81 tetraspanins, had not been shown previously to affect tumor behavior *in vivo*. Here, we show that EWI-2 is substantially downregulated on glioblastomas compared to normal brain. Furthermore, EWI-2 expression inhibits glioblastoma tumor growth *in vivo* while also inhibiting three-dimensional growth and invasion and migration *in vitro*. These inhibitory effects are accompanied by reorganization of tetraspanin-enriched membrane microdomain components (i.e., CD9 and CD81) as well as matrix metalloproteinases (i.e., MMP-2 and MT1-MMP) on the surface of glioblastoma cells.

Materials and Methods

Plasmids and Reagents

Monoclonal antibodies (mAbs) to CD9 (ALB6; Beckman Coulter, Hialeah, FL), CD63 (6H1), CD81 (M38), CD82 (M104), CD151 (5C11), MHC class I (W6/32), CD147 (8G6), and EWI-2 polyclonal antibody were referenced previously [3,4]. Anti–EWI-2 mAb 8A12 [18] was a gift from Dr. E. Rubinstein. The M2 anti-FLAG mAb, horseradish peroxidase–conjugated goat antimouse polyclonal antibody and nonimmune mouse IgG were from Sigma (St. Louis, MO). C-terminal FLAG-tagged EWI-2 and CD2 were described [2,3].

Gene Expression Data Analysis

Primary gene expression data were downloaded from the Gene Expression Omnibus Web site (http://www.ncbi.nlm.nih.gov/geo/) and used as is. From these data [19,20], notched box-and-whisker graphs were generated using the R graphics module (http://www.r-project.org/). The Henry Ford GEO Data Set (GSE4290, *top panel*) includes MAS5 signal intensities for nontumor and grades II to IV glioblastoma samples [20]. The Stanford GEO Data Set (GSE2223) is a $\log_2$ Cy5/Cy3 ratio for normal brain reference samples and grades II to IV glioblastoma samples [21,22]. For genes with multiple probes, data from all probes are included. Dashed lines indicate the median of all probes across all samples in each data set. Notches indicate 95% confidence intervals surrounding the median (dark line). The boxes denote the 25th to 75th percentiles, and the whiskers extend to 1.5 times the interquartile range of the data. Outliers are indicated as open circles. Significance was calculated by 2-tailed Welch's *T*-test.

Cell Culture and Retroviral Transduction

The human glioblastoma cell lines T98G and U87-MG (American Type Culture Collection (ATCC), Manassas, VA) and FNX-ampho packaging cells (ATCC) were maintained in Dulbecco's modified Eagle's medium (DMEM) with 10% fetal bovine serum (Invitrogen, Carlsbad, CA). Transient transfection of FNX-ampho cells and retroviral infection of T98G and U87-MG cells were performed as described [23]. Stable infectants were selected in a medium containing 200 μg/ml zeocin (Invitrogen) and were maintained as a polyclonal cell population. The U87-MG cells expressing luciferase-neomycin phosphotransferase (*neo*) fusion protein (U87-LucNeo cells) were previously described [24].

Metabolic Labeling, Immunoprecipitation, Immunoblot Analysis, and Zymography

For [^{3}H]palmitate labeling, U87-LucNeo cells at 80% to 90% confluence were serum-starved for 2 hours and then pulsed for 2 hours in medium containing 0.2 mCi/ml [^{3}H]palmitic acid (NEN Bioscience, Boston, MA) and 5% dialyzed FBS (Invitrogen). Metabolic labeling with [^{3}H]palmitate is an effective means of analyzing TEMs, which are palmitate-enriched [25]. Cells were then lysed in 1% Brij 99, and immunoprecipitations were carried out as described [3]. Proteins resolved by SDS-PAGE were transferred to polyvinylidene fluoride membrane (BioRad Laboratories, Hercules, CA) and exposed to BioMax MS film (Kodak, Rochester, NY) at −80°C with an intensifying screen, to detect [^{3}H]labeling. Nonradioactive samples were transferred to nitrocellulose membrane and immunoblotted as described [3]. A phosphoimager machine (Storm 860; Molecular Dynamics, Co., Sunnyvale, CA) together with ImageQuant v.1.2. program was used for densitometric scanning of selected protein bands.

For gelatin zymography, serum-free conditioned media from U87-LucNeo cells or washed beads containing purified protein complexes were mixed with SDS sample buffer and separated on 10% SDS-PAGE copolymerized with 1 mg/ml gelatin (Sigma). Zymograms were then washed twice in 50 mM Tris-HCl, 5 mM $CaCl_2$, pH 8.0, and 2.5% Triton X-100 for 1 hour and then incubated in 50 mM Tris-HCl, pH 7.5, 5 mM $CaCl_2$ overnight at 37°C. Gels were stained with Coomassie brilliant blue, and densitometry was performed on inverted (black on white) images as mentioned in the previous paragraph.

Cell Proliferation, Chemotactic Migration, and Matrigel Invasion Assays

To assess proliferation, cells (5×10^4) were plated in triplicate wells of 24-well plates and then, at various times, were fixed and stained with methylene blue, extracted, and quantitated at OD of 650 nm. For migration and Matrigel invasion assays, BD BioCoat growth factor reduced Matrigel invasion chambers (BD Biosciences, Bedford, MA) were used according to the manufacturers' instructions. Briefly, the transwell membrane filter inserts (6.5 mm in diameter, 8-μm pore size, 10-nm-thick polycarbonate membrane), either coated with Matrigel (invasion assays) or uncoated (migration assays), were placed in a 24-well tissue culture plates. Cells (3×10^4) suspended in serum-free DMEM containing 0.1% heat-inactivated BSA, were added to top chambers in triplicate, and DMEM containing 10% FBS was added to each bottom chamber. After an overnight incubation at 37°C, nonmigrating cells were removed from the upper face of the filter using cotton swabs, and cells on the lower filter surface were fixed and stained with Diff-Quick (Baxter Healthcare Corp., McGraw Park, IL). The number of cells per field was counted under a light microscope.

Soft Agar and In Vivo *Tumor Growth Assays*

T98G and U87-MG cells were plated, in six-well plates, in 0.35% agar in complete medium over a solid underlay of 0.55% agar. Colonies were counted after 3 to 4 weeks at 37°C in humidified conditions. To assess ectopic growth, T98G cells (4×10^6 cells per flank in 1:1 mixture of RPMI media were injected subcutaneously into both flanks of irradiated (4.5 Gy of total body radiation) male nude mice (Taconic, Germantown, NY). Tumors were monitored for 3 months and measured with calipers weekly.

Intracranial orthotopic xenografts were established by implanting 50,000 U87-LucNeo cells (± EWI-2) as described [24]. At 6- to 8-day intervals, mice were anesthetized, injected with D-luciferin and imaged with the IVIS Imaging System (Xenogen, Alameda, CA), as described [24]. All animal procedures were approved by the Dana-Farber Cancer Institute Animal Care and Use Committee.

Immunohistochemistry of Xenograft and Human Brain Samples

Primary human glioblastoma tumors (BT34, BT70, BT74, and BT79) were propagated in SCID mice in the brain and subcutaneously as described elsewhere [26]. These xenografts have the same genetic and immunohistochemical characteristics of the original tumor as reported in the literature [26,27] and confirmed in our own laboratory (S.K., unpublished results). Histologic screening of xenograft tumors (both primary and U87-MG cell lines) was performed by serial analysis of hematoxylin and eosin coronal sections taken at ~5-mm intervals along the entire brain. Normal brain samples were obtained from autopsy cases at Brigham and Women's Hospital. Collection and use of fresh and discarded human tumor tissue was approved through Brigham and Women's Hospital Institutional Review Board. Immunohistochemistry was performed according to standard protocols [28]. Rabbit anti–EWI-2 polyclonal antibody was incubated at 1:10,000 dilution for ~10 hours at 4°C. After incubation with peroxidase-conjugated secondary antibody for 45 minutes, peroxidase substrate (diaminobenzidine) was added for 5 minutes, and slides were counterstained with Mayer's hematoxylin for 2 minutes.

Statistics

Unless otherwise indicated, graphs show means ± SD and significance was calculated by 2-tailed Student's *T*-test, with unequal variance.

Results

EWI-2 Is Present in Normal Brain But Lost in Human Gliomas

In two independent human data sets, EWI-2 (IGSF8) mRNA was considerably diminished in grade II, grade III astrocytic tumors, and most significantly in grade IV astrocytoma, compared to normal brain (Figure 1*A*, *top and bottom panels*). Conversely, another member of the EWI protein family, EWI-F, was elevated in each type of astrocytoma, with the effect most obvious in grade IV glioblastoma (Figure 1*A*). In the same data sets, two other members of the EWI protein family (EWI-3 and EWI-101) and tetraspanin proteins (CD9 and CD81) were increased only slightly in high-grade astrocytic tumors compared to normal brain tissue (Figure W1). Another tetraspanin protein, CD151, which can associate indirectly with EWI-2 [4], was substantially increased in grade IV glioblastoma (Figure W1). In other experiments, EWI-2 mRNA was highly expressed throughout adult human brain (Figure W2), and abundant EWI-2 protein was stained in normal human brain (Figure 1*B*, *e*), especially in the cortex (c) more so than in white matter (w). By contrast, primary human glioblastoma tumors, propagated in mouse brains, showed minimal staining for EWI-2 (Figure 1*B*, *c* and *f*). Tissue sections in subpanels *c* and *f* of Figure 1*B* are representative of results from four different human glioblastoma tumors and subpanel *e* is representative of three different normal human brain samples. In control experiments, U87 tumors in mouse brain did not stain for EWI-2 (Figure 1*B*, *a*), whereas EWI-2–transfected U87 tumors were strongly positive (Figure 1*B*, *d*). Background staining with negative control antibody is shown for normal human brain (Figure 1*B*, *b*). Furthermore, EWI-2 protein, detected using anti–EWI-2 antibodies, is well expressed in normal human astrocytes in culture within total lysate (Figure W3*A*) and on the cell surface (Figure W3*B*). EWI-2 protein is also abundant in normal brain cortex, hippocampus, and cerebellum, as shown elsewhere [29–31]. Conversely, EWI-2 protein expression was undetectable in total cell lysate from glioblastoma cell lines U87 and T98G, unless cells had been transfected (Figure W3*C*). Similarly, EWI-2 protein was minimally detected on the surface of four different glioblastoma cell lines (Figure W4*A*) but could be seen on other cell types (Figure W4*B*). A summary of EWI-2 expression results (Table W1) indicates that EWI-2 RNA and protein is abundant in normal brain and in normal astrocytes. Conversely, EWI-2 RNA and protein is essentially absent from glioblastoma tumors and cell lines. From these results, we hypothesized that EWI-2 may inhibit astrocytoma growth *in vivo*. As an initial test of this hypothesis, Kaplan-Meier survival curves were generated from a combined grade III and grade IV glioblastoma patient data set. As indicated (Figure 1*C*), patients with low EWI-2 expression showed significantly diminished survival. Similar trends were seen when grade III and grade IV data sets were analyzed separately, although statistical significance was not achieved owing to the smaller numbers in each group (Figure W5).

EWI-2 Reexpression Inhibits Astrocytoma Growth In Vivo

To test more directly for possible *in vivo* antitumor effects of EWI-2, we expressed EWI-2 in T98G glioblastoma cells at a moderate level comparable that naturally occurring in HeLa cells (Figure W4*B*). Control and EWI-2–transfected cells were then injected subcutaneously into nude mice. Cells expressing CD2 or vector control formed tumors in ~50% of the mice, within 45 days. However, no tumors were observed (in eight mice), even after 90 days, when EWI-2 was present (Figure 2*A*). Having observed EWI-2 inhibition of glioblastoma growth in this preliminary subcutaneous xenograft model, we then proceeded to test EWI-2 effects in an orthotopic tumor growth model. U87-LucNeo cells expressing either control vector, or EWI-2, were injected intracranially, and tumor growth was quantified over time by noninvasive imaging of tumor-associated bioluminescence. Bioluminescence imaging is rapid, nonlethal, noninvasive, and closely correlated with volumetric measurements [24]. Every control mouse showed detectable tumor growth, as recorded by *in vivo* imaging (Figure 2*B*). By contrast, few tumors were seen in mice injected with U87-LucNeo/EWI-2 cells, and those seen were generally smaller (Figure 2*B*). Quantitation of results from three independent experiments confirmed that EWI-2, during a 20- to 40-day period, markedly suppressed orthotopic tumor formation by U87-LucNeo cells in mice

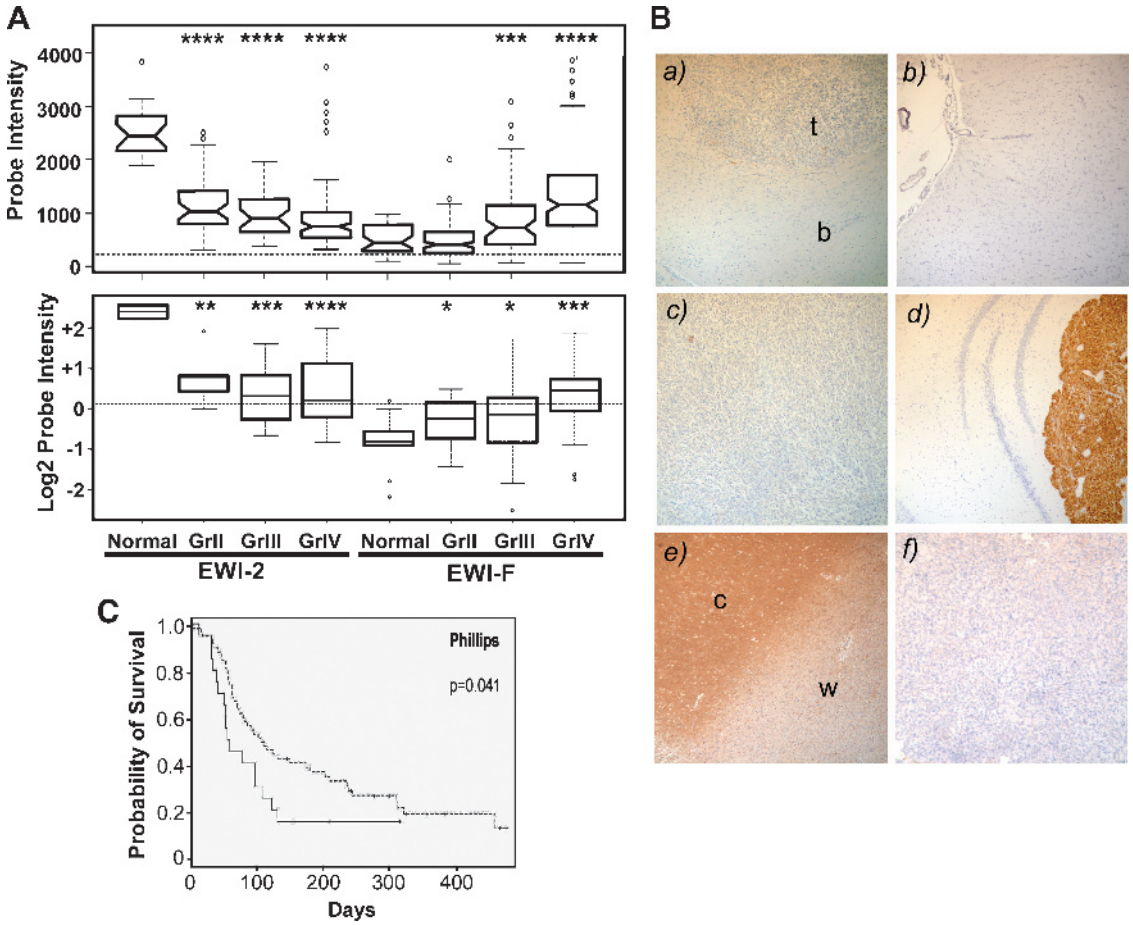

Figure 1. EWI-2 expression in human astrocytoma and normal brain. (A) EWI gene expression in normal human brain and astrocytoma (grades II, III, IV) samples. The Henry Ford GEO Data Set (GSE4290, top panel) includes 23 nontumor, 42 grade II, 31 grade III, and 77 grade IV glioblastoma samples. The Stanford GEO Data Set (GSE2223, bottom panel) includes 4 normal brain, 5 grade II, 9 grade III, and 27 grade IV glioblastoma samples. Molecules analyzed are EWI-2 (IGSF8, PGRL) and EWI-F (PTGFRN, CD9P-1, FPRP, CD315). (B) EWI-2 protein expression is shown in sections of (c) and (f) human glioblastoma tumors (representative of samples from four different tumors) and (e) normal human brain: c indicates cortex; w, white matter (representative of samples from three different brains). Control experiments show absence of EWI-2 staining in (a) U87 tumor = t, implanted in mouse brain = b; and presence of EWI-2 in (d) U87–EWI-2–transfected cells implanted in mouse brain; (b) negative control antibodies are used to show background staining in normal human brain. (C) *EWI-2* gene expression correlates with glioma patient survival. The Phillips data (GEO DataSet GSE4271) are MAS5 signal intensities for 77 grade III and grade IV glioblastomas [60]. The Phillips data were divided based on EWI-2 MAS5 expression values (probe set 225025_at) into above (n = 57, dashed line) or below (n = 20, solid line) first quartile groups. Censored data are indicated by vertical ticks. P value is the log rank test probability. Note: MAS5 is a statistical algorithm developed by Affymetrix, Inc. to estimate gene expression from array data, as described in a documentation available from Affymetrix.com.

(Figure 2*C*). Analysis of tissue slices from injected mice confirmed the bioluminescence imaging results. For example, in Figure 2*C*, experiment 3, tumors were present in 10 of 10 brains injected with control U87-LucNeo cells, whereas only 8 of 15 brains showed tumors on U87-LucNeo/EWI-2 injection, and those tumors were smaller. Representative brain sections from eight mice are shown in Figure W6. As indicated in Figure 2*D*, EWI-2 was expressed on the cell surface of U87-LucNeo cells at a level only 4.3-fold greater than endogenous EWI-2. Hence, excessive overexpression does not explain the effects of EWI-2 on orthotopic U87-LucNeo cell growth.

EWI-2 Inhibition of Glioblastoma Cell Functions In Vitro

To gain insight into how EWI-2 might be functioning *in vivo*, we carried out relevant *in vitro* assays using glioblastoma-derived cell lines T98G and U87-MG (or U87-LucNeo). Compared to controls, EWI-2 did not affect U87-LucNeo cell proliferation *in vitro* during a 2- to 6-day interval (Figure 3*A*). However, anchorage-independent growth in soft agar is typically seen as an assay more relevant to the *in vivo* behavior of transformed cells. In soft agar, both T98G and U87-MG cells showed significantly reduced colony formation on expression of EWI-2 but not vector or CD2 control protein (Figure 3*B*). Hence, EWI-2 can at least partially affect anchorage-independent growth of glioblastoma cells. Cell invasion and migration is also relevant to the progression of glioblastoma *in vivo* [32]. In this regard, expression of EWI-2 significantly diminished U87-LucNeo cell invasion and chemotactic migration 45% and 30%, respectively (Figure 3*C*). Hence, combined effects of EWI-2 on both anchorage-independent growth and tumor invasion/migration may explain glioblastoma inhibition *in vivo*.

EWI-2 Causes Reorganization of Its Associated Cell Surface Protein Complexes

Next, we sought to identify relevant molecular mechanisms to help explain EWI-2 function. Initially, we focused on tetraspanins CD9 and CD81 because 1) these molecules themselves may play critical roles during gliomagenesis (see the introduction), 2) they associate closely with EWI-2, and 3) they are known to regulate cell growth, migration, and invasion (see the introduction). For these studies, we focused on plasma membrane organization of CD9 and CD81 because this has been previously linked to EWI-2 function [3,4] and correlated with tumor cell malignancy [17]. Immunoprecipitation of either CD9 or CD81 from surface biotin-labeled U87-LucNeo cells yielded EWI-2 (Figure 4*A*). Hence, tetraspanin–EWI-2 complexes are present on the cell surface. Furthermore, the presence of EWI-2 caused staining with anti-CD9 mAb C9BB to decrease by ~70% relative to total CD9, stained by mAb MM2/57 (Figure 4*B*). The mAb C9BB preferentially recognizes homoclustered CD9 [17]. Consequently, EWI-2 is causing CD9 to become reorganized into heteroclusters, as seen previously in other cell types [17]. Tetraspanin reorganization could also be seen in immunoprecipitation experiments. Recoveries of CD81 (on CD9 immunoprecipitation) and CD9 (on CD81 immunoprecipitation) were markedly increased when EWI-2 was present in U87-LucNeo cells (Figure 4*C*). For example, as indicated by densitometric scanning (Figure 4*D*), approximately three-fold more CD81 associated with CD9, and approximately three-fold more CD9 associated with CD81 when EWI-2 was present (compare lanes 2 and 4 with lanes 1 and 3). Thus, the molecular organization of CD9 and CD81, with respect to neighboring proteins, is substantially affected by the presence of EWI-2 in these cells. In other experiments, we found that EWI-2 expression did not trigger any detectable shedding of either CD9 or CD81-containing complexes from intact cells into the growth media. In addition, EWI-2 expression did not affect tetraspanin internalization, during a 1- to 3-hour period, as assessed by monitoring the disappearance of cell surface–bound antibodies.

For further mechanistic insight into EWI-2 effects on glioblastoma, we focused on MMP-2 because 1) pericellular proteolysis, involving proteases such as MMP-2, plays a key role during glioblastoma invasion and survival [33–35] and 2) MMP-2 activation is supported by tetraspanins CD9 and CD81 (M.L. et al., manuscript submitted). On EWI-2 expression, there were no obvious changes in secreted MMP-2 levels, from U87-MG cells, at three different time points in a gelatin zymogram assay (Figure 5*A*). However, tetraspanin-associated MMP-2 was changed. Immunoprecipitation

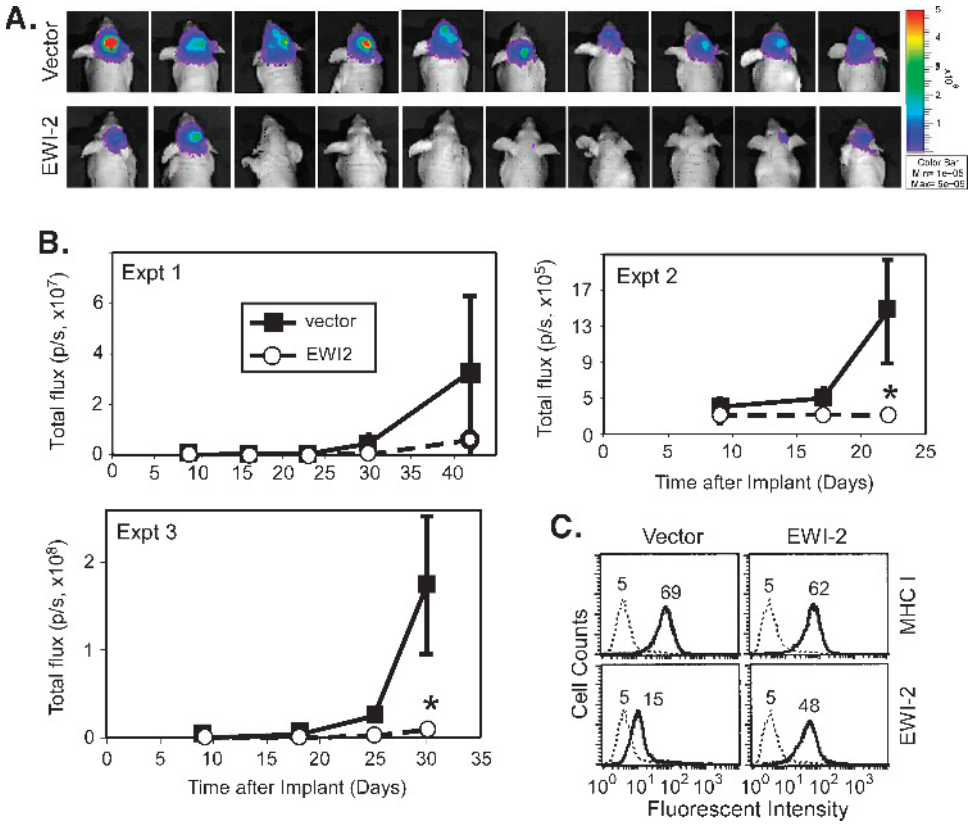

Figure 2. *In vivo* tumor formation. (A) T98G cells (4×10^6 cells) were injected subcutaneously into nude mice (in two flanks, four mice per cell line), and tumor sizes, (*l*)(*w*)(*h*)(0.52), were determined after 90 days. *$P < .05$ when EWI-2 samples are compared with vector control results. $P < .02$ when EWI-2 samples are compared with pooled control experiments (vector control plus CD2 control), according to Fisher exact test. (B) U87-LucNeo and U87-LucNeo/EWI-2 cells (50,000) were each injected intracranially into 10 nude mice and then imaged after 14 days. (C) Three independent experiments were carried out as in (B), and tumor size was quantitated by *in vivo* bioluminescence imaging (*$P < .05$). Note that tumors were observed in 100% of vector control mice. The arbitrary units representing photon flux values (*y*-axes) show interexperimental variability that may arise owing to the use of different stocks of luciferin, altered imaging parameters, altered size of the imaging area, or other variables. However, these parameters were carefully controlled intraexperimentally. (D) Cell surface expression of EWI-2 and control MHC class I in U87-LucNeo cells.

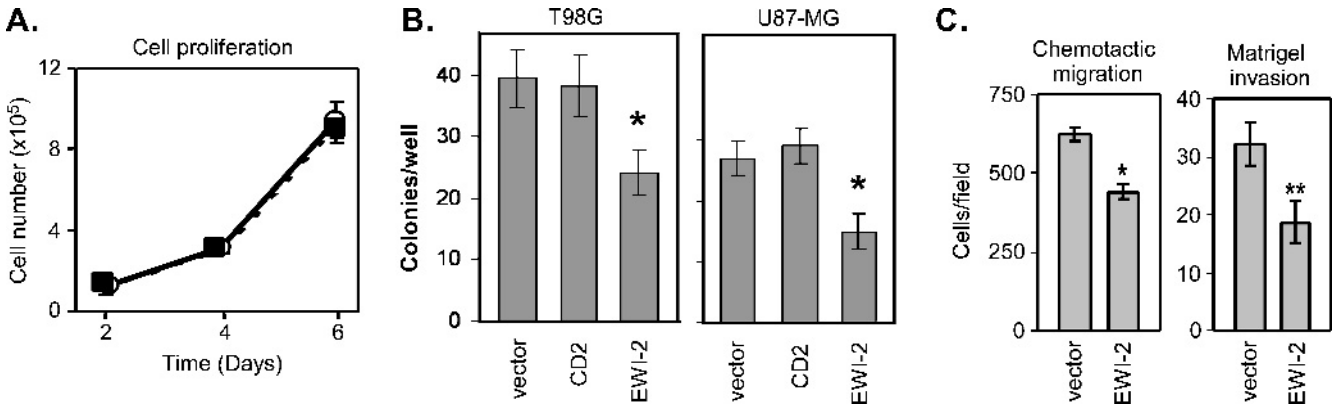

Figure 3. EWI-2 effects on proliferation, soft agar colony formation invasion and migration. (A) Cell numbers were measured for U87-LucNeo cells stably transduced with vector (open circles), or EWI-2 (closed squares). (B) The indicated cell lines expressing vector alone, CD2 (another cell surface IgSF protein), or EWI-2 were plated (600 cells per well) in soft agar for 3 weeks, and then colonies were counted (*$P < .01$ *vs* vector control cells). (C) U87-LucNeo cells, transduced with vector or EWI-2, were measured for chemotactic migration and cell invasion (*$P < .01$; **$P < .001$).

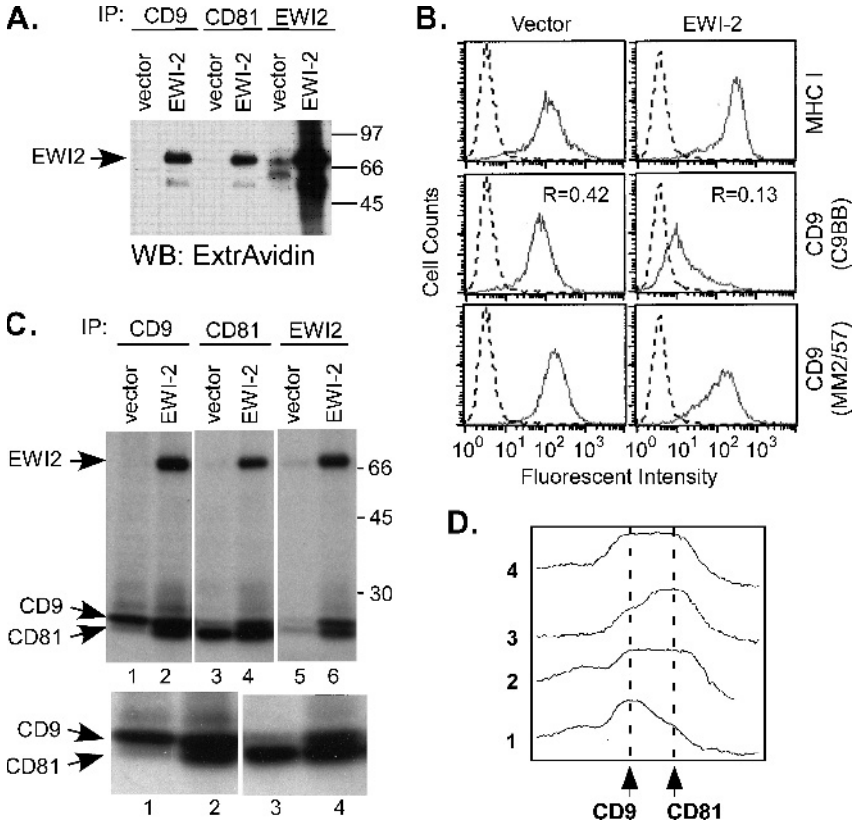

Figure 4. EWI-2 affects cell surface molecular organization of CD9 and CD81. (A) Intact U87-LucNeo cells (expressing wild type EWI-2 or vector control) were labeled with biotin and were then lysed. CD9, CD81, and EWI-2 were immunoprecipitated, and cell surface proteins were visualized by blot analysis with ExtrAvidin. Note: EWI-2–associated CD9 and CD81 themselves do not label very well with biotin because associated proteins limit accessibility (e.g., see Kolesnikova et al. [3]). (B) U87-LucNeo cells, expressing vector alone or EWI-2, were incubated with mAb W6/32 (to MHC-I), mAb C9BB (which preferentially recognizes oligomerized CD9 [18], or mAb MM2/57 (which recognizes total CD9). After washing, bound antibodies were visualized using fluorescein isothiocyanate–rabbit antimouse second antibody, and quantitated by flow cytometry. R = ratio of mean fluorescence intensities for C9BB divided by MM2/57. (C) U87-LucNeo cells, expressing vector alone or EWI-2, were labeled with ^{3}H-palmitate, lysed, and then CD9, CD81, and EWI-2 were immunoprecipitated. Lower panels show an enlarged view of key regions from the top panel. The palmitoylation of EWI-2 on membrane proximal cysteines will be described in more detail elsewhere. (D) Densitometric scans of lanes 1 to 4 are shown. Quantitation reveals increases of approximately three-fold in recovery of CD9 (in lane 4 *vs* 3) and CD81 (in lane 2 *vs* 1). Note: These results provide the first definitive demonstration that EWI-2 is palmitoylated.

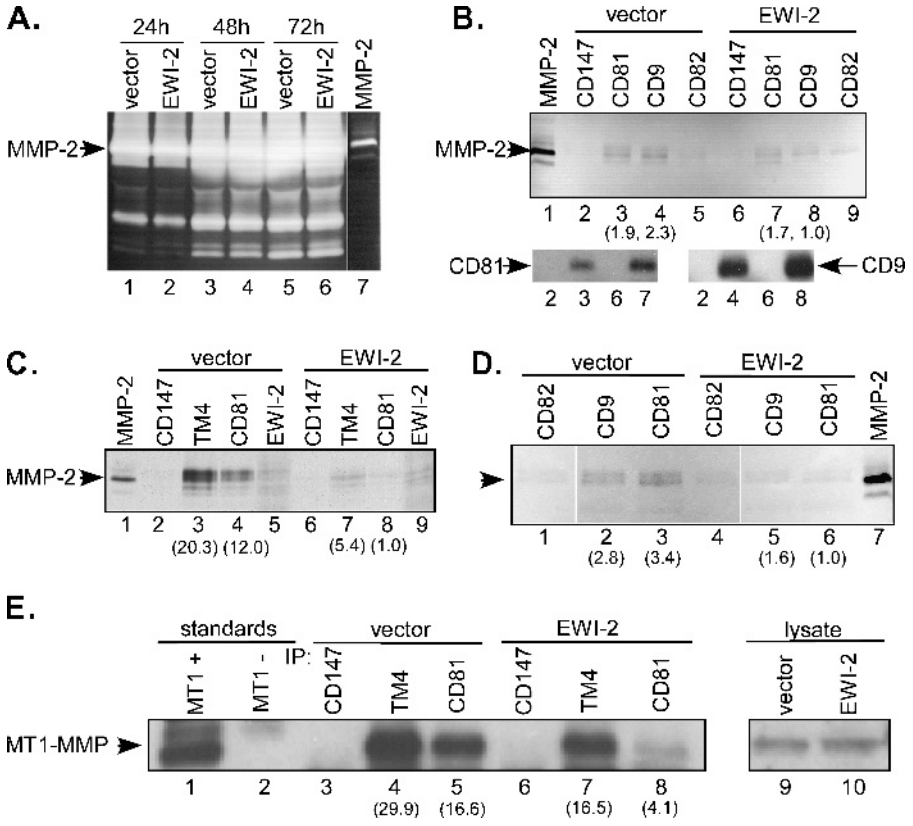

Figure 5. EWI-2 affects the molecular organization of MMP-2 and MT1-MMP. (A) Conditioned media were collected from U87-LucNeo cells (± EWI-2) and assayed for MMP-2 levels using gelatin zymography. (B, C) U87-LucNeo cells (± EWI-2) were lysed, protein complexes were immunoprecipitated, and associated MMP-2 levels were determined using gelatin zymography. TM4 = mixture of CD9, CD63, CD81, CD82, and CD151. Numbers in parentheses indicate relative amounts of MMP-2 in corresponding lanes. Selected samples (in B) were also analyzed for the presence of CD81 and CD9, as determined by Western blot analysis with M38 (CD81) and ALB6 (CD9) antibodies (lower panels). (D) T98G cells (± EWI-2) were lysed and analyzed as in (B, C). Note: Zymograms in (B–D) are inverted to show black on a white background. (E) U87-LucNeo cells (± EWI-2) were lysed, protein complexes were immunoprecipitated, and associated MT1-MMP levels were determined by immunoblot analysis of the active form of MT1-MMP. MT1-MMP in total lysates was also blotted. TM4 = mixture of CD9, CD63, CD81, CD82, and CD151. Numbers in parentheses indicate the relative amounts of MT1-MMP in the corresponding lanes. MT1-MMP standards are from MCF-7 cell lysates with or without MT1-MMP expression.

of pooled tetraspanins (Figure 5*C*, *lane 3*) or CD81 alone (*lane 4*) from mild detergent lysates of U87-LucNeo cells yielded MMP-2 gelatinolytic activity. Recovery of this activity was diminished by 70% to 90% when EWI-2 was present (Figure 5*C*, *lanes 7 and 8*). In additional experiments, MMP-2 activity associated with CD81 and CD9 was reduced by 13% to 57% in U87 cells (Figure 5*B*, *compare lanes 3 and 4 with 7 and 8*) and by 43% to 71% in T98G cells (Figure 5*D*, *compare lanes 2 and 3 with 5 and 6*) when EWI-2 was present. Diminished MMP-2 activity was not caused by the decreased immunoprecipitation of CD9 or CD81. In fact, recovery of CD9 and CD81 was typically increased when EWI-2 was present, as seen by immunoblot analysis (Figure 5*B*, *lower panels*; Figure 5*D*, not shown). Minimal amounts of MMP-2 were recovered on immunoprecipitation of CD147, an abundant cell surface protein that does not associate with TEMs (Figure 5, *B* and *C*, *lanes 2 and 6*), or of CD82, a tetraspanin that associates poorly with EWI-2 (Figure 5*B*, *lanes 5 and 9*; Figure 5*D*, *lanes 1 and 4*).

We suspected that a subset of total MMP-2 may be linked to tetraspanins through membrane-bound protease MT1-MMP because 1) MT1-MMP can associate with CD9 and CD81 (M.L. et al., manuscript submitted) and 2) MMP-2 is known to form a complex with MT1-MMP during MMP-2 activation [36]. Immunoprecipitation of pooled tetraspanins (Figure 5*E*, *lane 4*) or CD81 alone (Figure 5*E*, *lane 5*) yielded MT1-MMP protein. However, when EWI-2 was present in U87 cells, association of MT1-MMP with pooled tetraspanins was decreased by 45% (compare lane 4 with lane 7) and association with CD81 was decreased by 75% (compare lane 5 with lane 8). Meanwhile, in U87 cells, there was no decrease in either the amount of total MT1-MMP (Figure 5*E*, *lanes 9 and 10*) or in the amount of tetraspanin proteins (e.g., Figure 5*B*, *lower panels*).

In conclusion, results in this section show that EWI-2 markedly reorganizes multiple molecules (CD9, CD81, MMP-2, MT1-MMP) of likely importance during glioblastoma invasion and growth.

Discussion

EWI-2 protein and gene transcripts are abundant in normal brain tissue and in primary astrocyte cultures. However, EWI-2 protein is reduced in all glioblastoma tumors and cell lines analyzed, and EWI-2 transcripts are markedly reduced in glioblastoma and other gliomas, as seen from the analysis of two independent human data sets. By contrast, transcripts corresponding to other EWI protein family members are either strongly (EWI-F) or moderately (EWI-101, EWI-3) increased in human glioma data sets, compared to normal brain. Loss of EWI-2 expression is accompanied by diminished survival for grade

III and grade IV glioma patients. Furthermore, EWI-2 reexpression abolished T98G ectopic (subcutaneous) tumor growth *in vivo*, and considerably impaired intracranial U87-MG tumor growth *in vivo*, in nude mice. EWI-2 expression in glioblastoma cell lines also inhibited soft agar growth, invasion, and migration. These studies demonstrate that EWI-2 may have tumor suppressor–like properties in preclinical glioma models. However, the prognostic and clinical significance of EWI-2 loss of function still needs to be evaluated prospectively.

The *EWI-2* gene, which maps to 1q23.1, is not known to be specifically mutated or deleted in gliomas. Of possible relevance, partial or complete 1q monosomies have been observed in a few adult astrocytomas [37], and 1q21-41 trisomy is associated with a worse prognosis in pediatric anaplastic astrocytoma [37,38]. However, although chromosome 1q alterations appear only in a minority of cases, EWI-2 expression is markedly diminished in most adult gliomas. Hence, another mode of regulation, e.g., at the level of transcription, possibly through promoter methylation, may play a major role. As a cell surface transmembrane protein, EWI-2 is quite distinct from known glioblastoma tumor suppressors, which typically are intracellular molecules involved in signaling or cell cycle regulation [39]. One other transmembrane protein that could serve as a glioma tumor suppressor is coxsackie and adenovirus receptor (CAR). The expression of CAR is markedly reduced in high-grade astrocytomas, and CAR diminishes the size of U87-MG tumor xenografts [40].

Our *in vitro* studies provide several insights into the mechanism of EWI-2 action. First, although EWI-2 did not inhibit glioblastoma cell proliferation in two-dimensional culture, it significantly inhibited soft agar growth, consistent with EWI-2 being antitumorigenic. Second, EWI-2 caused a decrease in cell invasion and migration. This helps to explain how EWI-2 could affect *in vivo* glioblastoma progression, which is a highly invasive process [34,35]. Rodent glioblastoma xenograft models are sometimes criticized for not recapitulating invasive pathologic features of human glioblastoma multiforme (GBM) [41]. However, GBM arising from implanted U87 cells does show histopathologic features compatible with tumor invasion into nonneoplastic brain parenchyma [42]. EWI-2 inhibition of glioblastoma cell invasion and migration is consistent with previously observed inhibitory effects on motility, spreading, and ruffling in carcinoma and leukemia cell lines [3–5].

Our biochemical studies provide mechanistic insights into EWI-2 functions *in vivo* and *in vitro*. We focused on molecules that 1) directly or indirectly associate with EWI-2 and 2) are known to affect relevant functions of astrocytes and/or glioblastoma cells. Initially, we focused on tetraspanin proteins CD9 and CD81. For CD9 and CD81, EWI-2 (and EWI-F) are the most robust protein partners yet described [2,43–45], and CD9 and/or CD81 are required for EWI-2 cell surface expression and maturation [4]. EWI-2 associated with tetraspanins CD9 and CD81 on the surface of glioblastoma cells, thereby disrupting CD9 homo-oligomers and enhancing formation of CD9–CD81–EWI-2 complexes. Similar results have been seen on the expression of EWI-2 in other cell types [3,4,17]. Such changes could affect glioblastoma cell invasion and growth in multiple ways: 1) EWI-2 can cause redistribution of CD9 and CD81 to filopodia [4]. If a similar change occurs in glioblastoma, CD81 and CD9 would be well positioned to modulate tumor cell expansion into brain parenchyma, especially because CD9 can affect the dynamics of filopodia formation [46]. 2) Reorganization and redistribution of CD9 could potentially be accompanied by rearrangement of CD9 partner molecules, such as transforming growth factor α and heparin-binding EGF-like growth factor, which play major roles during glioblastoma tumor progression [6,11,12]. 3) Redistribution of CD9 and CD81 could lead to altered localization and function of CD9 and CD81-associated signaling molecules, such as protein kinase C [47] and PI 4-kinase [48]. 4) Alterations in CD9 and CD81 organization could affect the subcellular positioning and functions of integrins and other relevant molecules. For example, EWI-2 can markedly affect CD9 and CD81 colocalization with $\alpha_3\beta_1$ integrin in filopodia [4]. In this regard, $\alpha_3\beta_1$ integrin also plays an important role during glioblastoma invasion [49]. Also, other tetraspanin proteins such as CD151 [4] can associate with EWI-2–CD9–CD81 complexes, and CD151 is upregulated on glioblastoma cells (Figure W1 and [22]) and can stimulate glioblastoma motility and invasion [50]. Hence, CD151 could play an opposing role during inhibition of glioblastoma functions by overexpressed EWI-2. Several additional genes have been shown to be differentially expressed in correlation with GBM occurrence (e.g., [51]) and patient survival (e.g., [52]). It remains to be seen whether any of these gene products act in coordination with EWI-2.

We also analyzed the effects of EWI-2 expression on key proteases MMP-2 and MT1-MMP. Both are known to be involved in glioblastoma cell invasion, survival, and growth [33,35,53]. MT1-MMP promotes tumor growth by disrupting three-dimensional matrix growth control exerted on tumors [54]. On expression of EWI-2, total protein levels of MMP-2 and MT1-MMP were unaltered. However, there was a substantial decrease in both the amount of MMP-2 activity and the amount of MT1-MMP protein recovered in association with tetraspanin complexes. We show elsewhere that MT1-MMP can associate with tetraspanins CD9 and CD81 (M.L. et al., manuscript submitted). Although tetraspanin CD151 was not a prominent partner for MT1-MMP on glioblastoma cells (M.L. et al., manuscript submitted), CD151–MT1-MMP association was seen on endothelial cells [55]. During MMP-2 activation, it forms a complex with MT1-MMP and TIMP-2 [36]. The existence of this complex helps to explain the parallel dissociation of MMP-2 and MT1-MMP from tetraspanins on EWI-2 expression. Our current model is that MMP-2–MT1-MMP complexes associate preferentially with homo-oligomeric CD9 and/or CD81. When EWI-2 is present, there is a shift toward hetero-oligomeric complexes [17], accompanied by MMP dissociation (as shown here). If EWI-2 is disrupting MMP complexes, while driving CD81 and CD9 into the filopodia [4], this would likely influence glioblastoma invasion, survival, and/or growth. However, it remains to be determined whether EWI-2 causes reorganization of MMPs within filopodia.

Another possibility is that EWI-2 inhibition of glioblastoma depends on EWI-2 interaction with a counter-receptor. So far, we have failed to identify potential counter-receptor activity, or specific counter-receptors, on astrocytoma cells. Nonetheless, a possible contribution by a counter-receptor cannot be ruled out.

In conclusion, we find that EWI-2 levels are considerably diminished in human glioblastoma samples in association with diminished patient survival. Furthermore, reexpression of EWI-2 in glioblastoma cell lines leads to impaired tumor growth *in vivo*, in both ectopic and orthotopic models. EWI-2 seems to function, at least in part, by extensively reorganizing CD9 and CD81 protein complexes. This is likely accompanied by concurrent reorganization of additional other CD9 and CD81 partner proteins (e.g., proteases, adhesion receptors, signaling molecules), thus leading to suboptimal glioblastoma growth, invasion, and motility. Finally, we speculate that the tumor suppressor effects of CD9 observed on several non–glioma tumor

types [56–58] could, to a large extent, involve inhibitory effects of EWI-2, which is CD9's major partner protein.

Acknowledgments

The authors thank Renee D. Wright for technical assistance with animal studies.

References

[1] *Brain Tumor Invasion. Biological, Clinical, and Therapeutic Considerations.* In T Mikkelsen, R Bjerkvig, OD Laerum, ML Rosenblum (Eds). ISBN: 978-0-471-15452-5.

[2] Stipp CS, Kolesnikova TV, and Hemler ME (2001). EWI-2 is a major CD9 and CD81 partner, and member of a novel Ig protein subfamily. *J Biol Chem* **276**, 40545–40554.

[3] Kolesnikova TV, Stipp CS, Rao RM, Lane WS, Luscinskas FW, and Hemler ME (2004). EWI-2 modulates lymphocyte integrin alpha4beta1 functions. *Blood* **103**, 3013–3019.

[4] Stipp CS, Kolesnikova TV, and Hemler ME (2003). EWI-2 regulates {alpha}3{beta}1 integrin-dependent cell functions on laminin-5. *J Cell Biol* **163**, 1167–1177.

[5] Zhang XA, Lane WS, Charrin S, Rubinstein E, and Liu L (2003). EWI2/PGRL associates with the metastasis suppressor KAI1/CD82 and inhibits the migration of prostate cancer cells. *Cancer Res* **63**, 2665–2674.

[6] Kawashima M, Doh-ura K, Mekada E, Fukui M, and Iwaki T (2002). CD9 expression in solid non-neuroepithelial tumors and infiltrative astrocytic tumors. *J Histochem Cytochem* **50**, 1195–1203.

[7] Kelic S, Levy S, Suarez C, and Weinstein DE (2001). CD81 regulates neuron-induced astrocyte cell-cycle exit. *Mol Cell Neurosci* **17**, 551–560.

[8] Geisert EE Jr, Williams RW, Geisert GR, Fan L, Asbury AM, Maecker HT, Deng J, and Levy S (2002). Increased brain size and glial cell number in CD81-null mice. *J Comp Neurol* **453**, 22–32.

[9] Nakamura K, Iwamoto R, and Mekada E (1995). Membrane-anchored heparin-binding EGF-like growth factor (HB-EGF) and diptheria toxin receptor–associated protein (DRAP27)/CD9 form a complex with integrin $\alpha_3\beta_1$ at cell-cell contact sites. *J Cell Biol* **129**, 1691–1705.

[10] Shi W, Fan H, Shum L, and Derynck R (2000). The tetraspanin CD9 associates with transmembrane TGF-alpha and regulates TGF-alpha–induced EGF receptor activation and cell proliferation. *J Cell Biol* **148**, 591–602.

[11] Mishima K, Higashiyama S, Asai A, Yamaoka K, Nagashima Y, Taniguchi N, Kitanaka C, Kirino T, and Kuchino Y (1998). Heparin-binding epidermal growth factor–like growth factor stimulates mitogenic signaling and is highly expressed in human malignant gliomas. *Acta Neuropathol* **96**, 322–328.

[12] Rubenstein M, Glick R, Lichtor T, Mirochnik Y, Chou P, and Guinan P (2001). Treatment of the T98G glioblastoma cell line with antisense oligonucleotides directed toward mRNA encoding transforming growth factor-alpha and the epidermal growth factor receptor. *Med Oncol* **18**, 121–130.

[13] Hemler ME (2003). Tetraspanin proteins mediate cellular penetration, invasion and fusion events, and define a novel type of membrane microdomain. *Ann Rev Cell Dev Biol* **19**, 397–422.

[14] Maecker HT, Todd SC, and Levy S (1997). The tetraspanin superfamily: molecular facilitators. *FASEB J* **11**, 428–442.

[15] Hemler ME (2005). Tetraspanin functions and associated microdomains. *Nat Rev Mol Cell Biol* **6**, 801–811.

[16] Le Naour F, Andre M, Greco C, Billard M, Sordat B, Emile JF, Lanza F, Boucheix C, and Rubinstein E (2006). Profiling of the tetraspanin web of human colon cancer cells. *Mol Cell Proteomics* **5**, 845–857.

[17] Yang XH, Kovalenko OV, Kolesnikova TV, Andzelm MM, Rubinstein E, Strominger JL, and Hemler ME (2006). Contrasting effects of EWI proteins, integrins, and protein palmitoylation on cell surface CD9 organization. *J Biol Chem* **281**, 12976–12985.

[18] Charrin S, Le Naour F, Labas V, Billard M, Le Caer JP, Emile JF, Petit MA, Boucheix C, and Rubinstein E (2003). EWI-2 is a new component of the tetraspanin web in hepatocytes and lymphoid cells. *Biochem J* **373** (Pt 2), 409–421.

[19] Liang Y, Diehn M, Watson N, Bollen AW, Aldape KD, Nicholas MK, Lamborn KR, Berger MS, Botstein D, Brown PO, et al. (2005). Gene expression profiling reveals molecularly and clinically distinct subtypes of glioblastoma multiforme. *Proc Natl Acad Sci USA* **102**, 5814–5819.

[20] Sun L, Hui AM, Su Q, Vortmeyer A, Kotliarov Y, Pastorino S, Passaniti A, Menon J, Walling J, Bailey R, et al. (2006). Neuronal and glioma-derived stem cell factor induces angiogenesis within the brain. *Cancer Cell* **9**, 287–300.

[21] Bredel M, Bredel C, Juric D, Duran GE, Yu RX, Harsh GR, Vogel H, Recht LD, Scheck AC, and Sikic BI (2006). Tumor necrosis factor-alpha–induced protein 3 as a putative regulator of nuclear factor-kappaB–mediated resistance to O^6-alkylating agents in human glioblastomas. *J Clin Oncol* **24**, 274–287.

[22] Bredel M, Bredel C, Juric D, Harsh GR, Vogel H, Recht LD, and Sikic BI (2005). Functional network analysis reveals extended gliomagenesis pathway maps and three novel MYC-interacting genes in human gliomas. *Cancer Res* **65**, 8679–8689.

[23] Pear W, Nolan G, Scott M, and Baltimore D (1993). Production of high-titer helper-free retroviruses by transient transfection. *Proc Natl Acad Sci USA* **90**, 8392–8396.

[24] Rubin JB, Kung AL, Klein RS, Chan JA, Sun Y, Schmidt K, Kieran MW, Luster AD, and Segal RA (2003). A small-molecule antagonist of CXCR4 inhibits intracranial growth of primary brain tumors. *Proc Natl Acad Sci USA* **100**, 13513–13518.

[25] Yang X, Kovalenko OV, Tang W, Claas C, Stipp CS, and Hemler ME (2004). Palmitoylation supports assembly and function of integrin-tetraspanin complexes. *J Cell Biol* **167**, 1231–1240.

[26] Giannini C, Sarkaria JN, Saito A, Uhm JH, Galanis E, Carlson BL, Schroeder MA, and James CD (2005). Patient tumor *EGFR* and *PDGFRA* gene amplifications retained in an invasive intracranial xenograft model of glioblastoma multiforme. *Neuro Oncol* **7**, 164–176.

[27] Singh SK, Hawkins C, Clarke ID, Squire JA, Bayani J, Hide T, Henkelman RM, Cusimano MD, and Dirks PB (2004). Identification of human brain tumour initiating cells. *Nature* **432**, 396–401.

[28] Ligon KL, Huillard E, Mehta S, Kesari S, Liu H, Alberta JA, Bachoo RM, Kane M, Louis DN, DePinho RA, et al. (2007). Olig2-regulated lineage-restricted pathway controls replication competence in neural stem cells and malignant glioma. *Neuron* **53**, 503–517.

[29] Murdoch J, Doudney K, Gerrelli D, Wartham N, Patermott C, Stanier P, and Copp A (2003). Genomic organization and embryonic expression of Igsf8, an immunoglobulin superfamily member implicated in development of the nervous system and organ epithelia. *Mol Cell Neurosci* **22**, 62–74.

[30] Olsen JV, Nielsen PA, Andersen JR, Mann M, and Wisniewski JR (2007). Quantitative proteomic profiling of membrane proteins from the mouse brain cortex, hippocampus, and cerebellum using the HysTag reagent: mapping of neurotransmitter receptors and ion channels. *Brain Res* **1134**, 95–106.

[31] Yamada O, Tamura K, Yagihara H, Isotani M, Washizu T, and Bonkobara M (2006). Neuronal expression of keratinocyte-associated transmembrane protein-4, KCT-4, in mouse brain and its up-regulation by neurite outgrowth of Neuro-2a cells. *Neurosci Lett* **392**, 226–230.

[32] Nakada M, Nakada S, Demuth T, Tran NL, Hoelzinger DB, and Berens ME (2007). Molecular targets of glioma invasion. *Cell Mol Life Sci* **64**, 458–478.

[33] Belkaid A, Fortier S, Cao J, and Annabi B (2007). Necrosis induction in glioblastoma cells reveals a new "bioswitch" function for the MT1-MMP/G6PT signaling axis in proMMP-2 activation *versus* cell death decision. *Neoplasia* **9**, 332–340.

[34] Lakka SS, Gondi CS, and Rao JS (2005). Proteases and glioma angiogenesis. *Brain Pathol* **15**, 327–341.

[35] Tysnes BB and Mahesparan R (2001). Biological mechanisms of glioma invasion and potential therapeutic targets. *J Neurooncol* **53**, 129–147.

[36] Seiki M (1999). Membrane-type matrix metalloproteinases. *APMIS* **107**, 137–143.

[37] Thiel G, Lozanova T, Vogel S, Kintzel D, Janisch W, and Witkowski R (1993). Age-related nonrandom chromosomal abnormalities in human low-grade astrocytomas. *Hum Genet* **91**, 547–550.

[38] Rickert CH, Strater R, Kaatsch P, Wassmann H, Jurgens H, Dockhorn-Dworniczak B, and Paulus W (2001). Pediatric high-grade astrocytomas show chromosomal imbalances distinct from adult cases. *Am J Pathol* **158**, 1525–1532.

[39] Ohgaki H (2005). Genetic pathways to glioblastomas. *Neuropathology* **25**, 1–7.

[40] Huang KC, Altinoz M, Wosik K, Larochelle N, Koty Z, Zhu L, Holland PC, and Nalbantoglu J (2005). Impact of the coxsackie and adenovirus receptor (CAR) on glioma cell growth and invasion: requirement for the C-terminal domain. *Int J Cancer* **113**, 738–745.

[41] Gutmann DH, Maher EA, and Van Dyke T (2006). Mouse models of human cancers consortium workshop on nervous system tumors. *Cancer Res* **66**, 10–13.

[42] Candolfi M, Curtin JF, Nichols WS, Muhammad AG, King GD, Pluhar GE, McNiel EA, Ohlfest JR, Freese AB, Moore PF, et al. (2007). Intracranial glioblastoma models in preclinical neuro-oncology: neuropathological characterization and tumor progression. *J Neurooncol* **85**, 133–148.

[43] Charrin S, Le Naour F, Oualid M, Billard M, Faure G, Hanash SM, Boucheix C, and Rubinstein E (2001). The major CD9 and CD81 molecular partner. Identification and characterization of the complexes. *J Biol Chem* **276**, 14329–14337.

[44] Clark KL, Zeng Z, Langford AL, Bowen SM, and Todd SC (2001). Pgrl is a major CD81-associated protein on lymphocytes and distinguishes a new family of cell surface proteins. *J Immunol* **167**, 5115–5121.

[45] Stipp CS, Orlicky D, and Hemler ME (2001). FPRP: a major, highly stoichiometric, highly specific CD81 and CD9-associated protein. *J Biol Chem* **276**, 4853–4862.

[46] Runge KE, Evans JE, He ZY, Gupta S, McDonald KL, Stahlberg H, Primakoff P, and Myles DG (2007). Oocyte CD9 is enriched on the microvillar membrane and required for normal microvillar shape and distribution. *Dev Biol* **304**, 317–325.

[47] Zhang XA, Bontrager AL, and Hemler ME (2001). TM4SF proteins associate with activated PKC and link PKC to specific beta1 integrins. *J Biol Chem* **276**, 25005–25013.

[48] Yauch RL and Hemler ME (2000). Specific interactions among transmembrane 4 superfamily (TM4SF) proteins and phosphatidylinositol 4-kinase. *Biochem J* **351**, 629–637.

[49] Chintala SK, Sawaya R, Gokaslan ZL, and Rao JS (1996). Modulation of matrix metalloproteinase-2 and invasion in human glioma cells by $\alpha_3\beta_1$ integrin. *Cancer Lett* **103**, 201–208.

[50] Kohno M, Hasegawa H, Miyake M, Yamamoto T, and Fujita S (2002). CD151 enhances cell motility and metastasis of cancer cells in the presence of focal adhesion kinase. *Int J Cancer* **97**, 336–343.

[51] Scrideli CA, Carlotti CG Jr, Okamoto OK, Andrade VS, Cortez MA, Motta FJ, Lucio-Eterovic AK, Neder L, Rosemberg S, Oba-Shinjo SM, et al. (2008). Gene expression profile analysis of primary glioblastomas and non-neoplastic brain tissue: identification of potential target genes by oligonucleotide microarray and real-time quantitative PCR. *J Neurooncol* **88**, 281–291.

[52] Marko NF, Toms SA, Barnett GH, and Weil R (2008). Genomic expression patterns distinguish long-term from short-term glioblastoma survivors: a preliminary feasibility study. *Genomics* **91**, 395–406.

[53] Nakada M, Okada Y, and Yamashita J (2003). The role of matrix metalloproteinases in glioma invasion. *Front Biosci* **8**, e261–e269.

[54] Hotary K, Li XY, Allen E, Stevens SL, and Weiss SJ (2006). A cancer cell metalloprotease triad regulates the basement membrane transmigration program. *Genes Dev* **20**, 2673–2686.

[55] Yanez-Mo M, Barreiro O, Gonzalo P, Batista A, Megias D, Genis L, Sachs N, Sala-Valdes M, Alonso MA, Montoya MC, et al. (2008). MT1-MMP collagenolytic activity is regulated through association with tetraspanin CD151 in primary endothelial cells. *Blood* **112**, 3217–3226.

[56] Huang CL, Liu D, Masuya D, Kameyama K, Nakashima T, Yokomise H, Ueno M, and Miyake M (2004). MRP-1/CD9 gene transduction downregulates Wnt signal pathways. *Oncogene* **23**, 7475–7483.

[57] Ovalle S, Gutierrez-Lopez MD, Olmo N, Turnay J, Lizarbe MA, Majano P, Molina-Jimenez F, Lopez-Cabrera M, Yanez-Mo M, Sanchez-Madrid F, et al. (2007). The tetraspanin CD9 inhibits the proliferation and tumorigenicity of human colon carcinoma cells. *Int J Cancer* **121**, 2140–2152.

[58] Miyake M, Nakano K, Ieki Y, Adachi M, Huang C-L, Itoi S, Koh T, and Taki T (1995). Motility related protein 1 (MRP-1/CD9) expression: inverse correlation with metastases in breast cancer. *Cancer Res* **55**, 4127–4131.

[59] Phillips HS, Kharbanda S, Chen R, Forrest WF, Soriano RH, Wu TD, Misra A, Nigro JM, Colman H, Soroceanu L, et al. (2006). Molecular subclasses of high-grade glioma predict prognosis, delineate a pattern of disease progression, and resemble stages in neurogenesis. *Cancer Cell* **9**, 157–173.

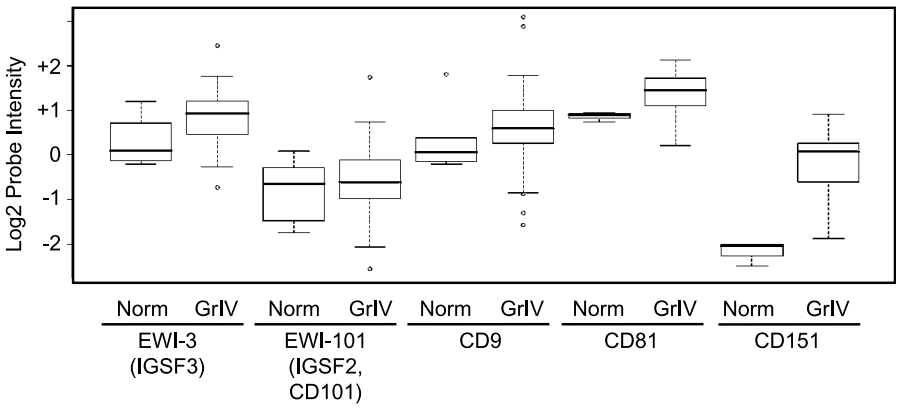

Figure W1. Expression of EWI proteins and tetraspanins in normal brain and in grade IV astrocytoma. Data shown are from the Stanford GEO DataSet GSE2223, analyzed as in Figure 1*A*, *bottom panel*. Molecules analyzed are EWI-3 (IGSF3), EWI-101 (CD101), CD9, CD81, and CD151. Similar results were obtained on analysis of these same molecules in the Henry Ford GEO Data Set (GSE4290, used in Figure 1*A*, *top panel*; not shown).

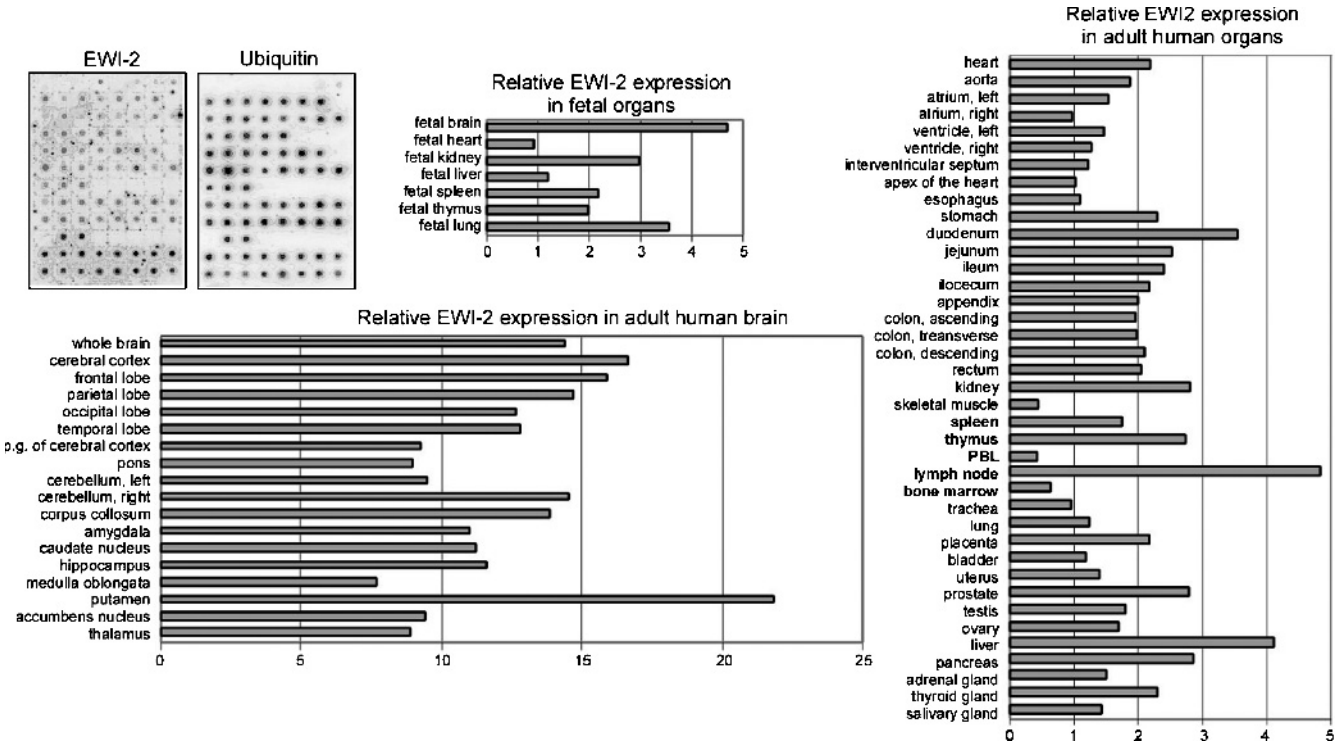

Figure W2. EWI-2 expression in diverse human tissues and organs. Multiple tissue expression array (Clontech, Mountain View, CA) was hybridized with EWI-2 probe or ubiquitin probe. Relative expression level of EWI-2 after normalization for ubiquitin probe is shown.

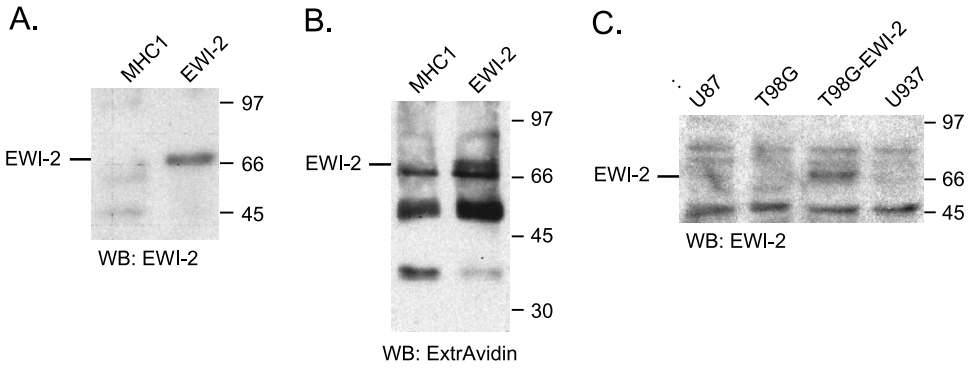

Figure W3. EWI-2 expression by normal human astrocytes. Normal human astrocytes (Lonza, Walkersville, Inc) were cell surface–labeled with biotin, lysed in 1% NP-40 and then MHC I (mAb W6/32) and EWI-2 (polyclonal antibody) were immunoprecipitated. Proteins were resolved by 10% SDS-PAGE and then blotted (A) using anti–EWI-2 mAb 8A12 to detect total immunoprecipitated EWI-2 or (B) ExtrAvidin to detect surface-biotinylated EWI-2. (C) Control cell lysates from U87, T98G, T98G−EWI-2, and U937 cells were blotted using anti–EWI-2 mAb 8A12.

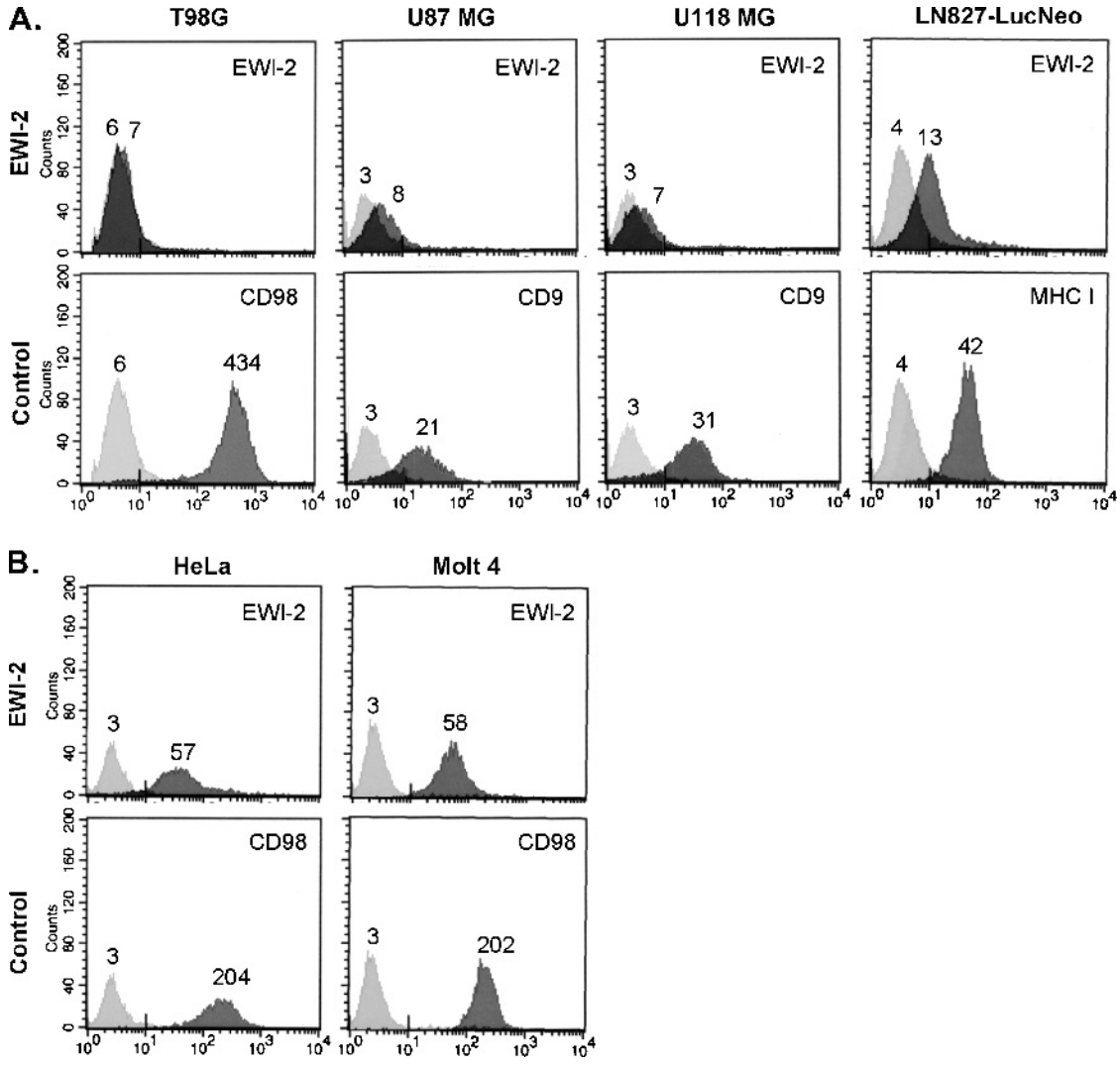

Figure W4. Cell surface expression of EWI-2 and control cell surface antigens (CD98, MHC class I, or CD9) in glioblastoma (A) and other cell lines (B). Cell lines used were glioblastoma cell lines T98G, U87 MG, U118 MG, and LN827-LucNeo, as well as Molt 4 (T cell leukemic cell line) and HeLa (ovarian carcinoma). Numbers next to peaks indicate mean fluorescence intensities.

Table W1. Summary of EWI-2 Expression Data.

Experiment	Normal Brain	Glioblastoma
RNA expression (Henry Ford GEO Data Set; Figure 1*A*, *top panel*)	++	–
RNA expression (Stanford GEO Data Set; Figure 1*A*, *bottom panel*)	++	–
RNA expression (Figure W2)	++	ND
RNA in developing mouse brain [29]	++	ND
RNA in adult mouse brain [31]	++	ND
Protein staining (IHC; Figure 1*B*)	++ (n = 3)	– (n = 4)
Protein on surface of human GBM cell lines (Figure W4)	ND	– (n = 4)
Protein in human GBM cell lysates (Figure W3*C*)	ND	– (n = 2)
Protein in primary human astrocytes (Figure W3, *A* and *B*)	++	ND
Protein in mouse brain [30]	++	ND

IHC indicates immunohistochemistry; ND, Not Determined

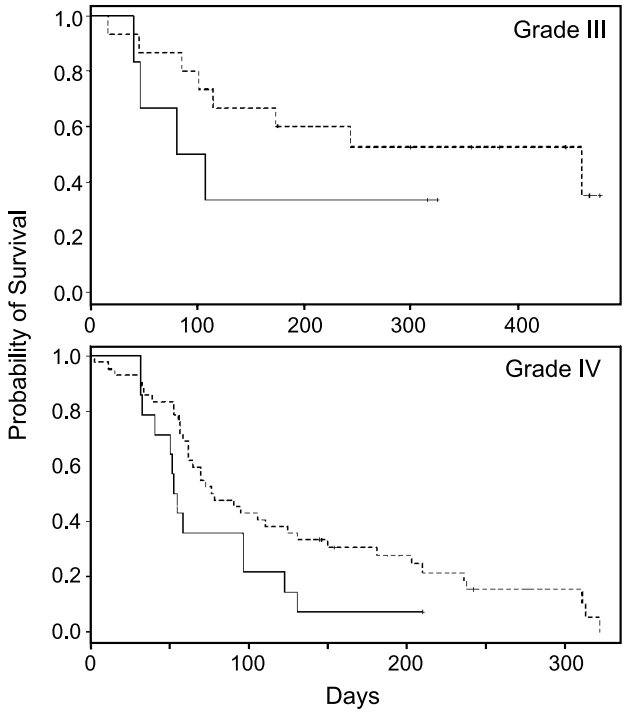

Figure W5. EWI-2 expression correlates with patient survival for both Grade III and grade IV glioblastomas. Data are analyzed exactly as in Figure 1*C*, except that grade III and grade IV glioblastomas are now analyzed separately, instead of being pooled. For grade III results, $P = .27$; for grade IV, $P = .057$. As indicated in Figure 1*C* for pooled results, $P = .041$.

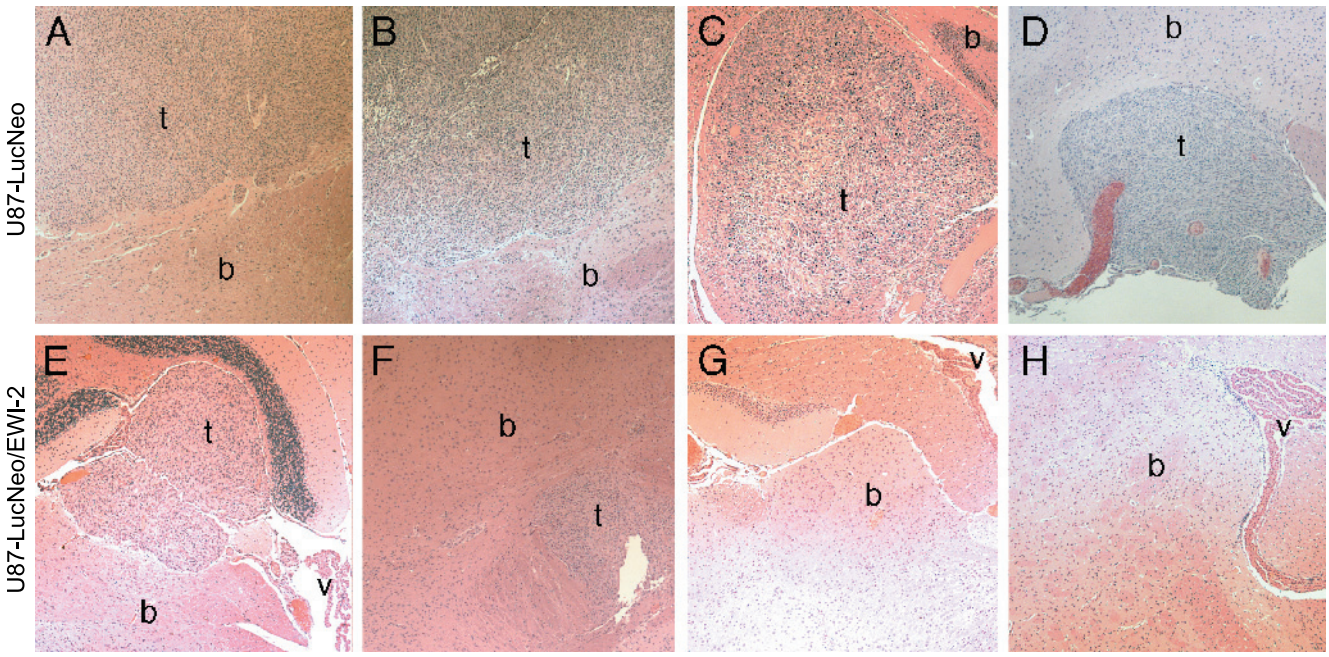

Figure W6. U87-LucNeo (A–D) and U87-LucNeo/EWI-2 (E–H) cells were injected intracranially as in Figure 1*C*. After 35 days, serial brain sections were obtained, starting from the injection point. All images show hematoxylin and eosin staining at 4× magnification. Sections are shown from four representative mice injected with U87-LucNeo control cells (top row) and four representative mice injected with U87-LucNeo/EWI-2 cells (bottom row). b indicates brain; t, tumor; v, ventricle.